STRUCTURAL, ELECTRONIC AND VIBRATIONAL STUDY OF 4, 6-DICHLORO-5-METHYLPYRIMIDINE: A DFT APPROACH

Bhawani Datt Joshi

Journal of Institute of Science and Technology

Volume 22, Issue 1, July 2017

ISSN: 2469-9062 (print), 2467-9240 (e)

JIST, **22** (1): 51-60 (2017)

Published by:

Institute of Science and Technology

Tribhuvan University

Kirtipur, Kathmandu, Nepal

JIST 2017, 22 (1): 51-60
ISSN: 2469-9062 (p), 2467-9240 (e)

Research Article

STRUCTURAL, ELECTRONIC AND VIBRATIONAL STUDY OF 4, 6-DICHLORO-5-METHYLPYRIMIDINE: A DFT APPROACH

Bhawani Datt Joshi
Department of Physics, Tribhuvan University, Siddhanath Sc. Campus, Mahendranagar, Nepal
Corresponding E-mail: pbdjoshi@gmail.com

ABSTRACT

Molecular structure, molecular electrostatic potential (MEP) and theoretical vibrational spectra of 4, 6-dichloro-5-methylpyrimidine (DMP) molecule have been presented in this paper. The vibrational spectra were calculated for monomer, dimer and unit cell DMP molecule using density function theory (DFT) and *ab initio* Hartree-Fock (HF) (for monomer) method employing 6-311++G (d, p) basis set using Gaussian 09 program. The frequencies obtained by DFT have smaller values than obtained from HF due to the inclusion of electron correlation in the previous one. Electronic absorption calculations are performed both in the gas and solvent phase using TD-DFT (including IEF-PCM model) to understand the stability, charge transfer and frontier molecular orbital energy gap. Large value of energy gap leads to the stability of molecule. Overlapping between calculated and the experimental structure show that the optimized geometry reproduced exactly similar structure as by the experiment.

Keywords: DMP, DFT, Vibrational spectra, MEP, IEF-PCM model.

INTRODUCTION

Nitrogen containing molecules have their wide medicinal applications. Pyrimidine derivatives containing nitrogen atoms are known for their pharmacological applications. They are used as pesticides, pharmaceutical agents (Condon *et al*., 1993; Maeno *et al*., 1990), antiviral agents (Alam *et al*., 2010), herbicides (Selby *et al*., 2002), antioxidant and for applications of organoselenide compounds (Khidre *et al*., 2013).The aim of present study is to investigate the vibrational frequencies of with potential energy distribution 4, 6-dichloro-5-methylpyrimidine (DMP) together with the structural parameters. X-ray diffraction method is one of the most frequently applied techniques for structural characterization of pharmaceutical compounds which is sensible to the long-range order molecules. Nowadays, there has been increasing attention for the application of vibrational spectroscopy (Raman and infrared) for non-destructive characterization of substance having short-range molecular structure (Srivastava *et al*., 2013). The quantum mechanical methods are strongly supporting theoretical tools. Vibrational spectroscopy is a valuable method for studying the dynamical behavior and to gain insight into the electronic structures of macromolecules at microscopic level (Srivastava *et al*., 2013; Mishra *et al*., 2014). They have been widely used to study the energetic, thermal and dynamical behavior from vibrational dynamics of large number of molecules/ or biomolecules.

The crystalline structure of DMP was recently elucidated by Medjani *et al*. (2015). It crystallizes in a monoclinic system belonging to the $P2_1/n$ space group with the crystal parameters: a = 7.463 (5), b = 7.827 (5), c = 11.790 (5) Å and β = 93.233 (5)º. The crystalline packing is governed by strong intermolecular hydrogen bonds involving both carbon (doner) and nitrogen (as acceptor) and forming inversion dimers. The crystal structure of DMP molecule is shown in figure 1 (a).

We have presented the vibrational modes of DMP for its monomer, dimer and the unit cell level using density functional theory (DFT) together with *ab initio* Hartree Fock (HF) theory. Further, MEP and electronic absorption in gas as well as in the solvent phase together with HOMO-LUMO analysis has been included.

MATERIALS AND METHOD

Computational details

The hybrid density functional theory (DFT) (Hohenberg & Kohn, 1964) calculations were

mainly carried out in the frame-work of the Becke–Lee–Yang–Parr (B3LYP) functional, in which the exchange functional is a local spin density exchange with Becke gradient correction (Casida & Chong, 1995) and the correlation functional is that of Lee, Yang and Parr with both local and non-local terms (Casida *et al*., 1998; Lee *et al*., 1988). Molecular geometry, vibrational frequencies and energies of optimized structures of the DMP were calculated employing 6-311++G (d, p) basis set (Becke, 1993; Parr & Yang, 1989) using Gaussian 09 (Frisch *et al*., 2009) program package. The vibrational assignments of the normal modes were made on the basis of the band profile, intensity and PED, calculated along the internal coordinates employing localized symmetry using GAR2PED program (Martin & Aslenov, 1995). For the molecule, isoelectronic molecular electrostatic potential surfaces (MEP) were calculated and plotted by the Gauss View program (Frisch *et al*. 2000) using DFT B3LYP/6-311++G (d, p) basis set.

RESULTS AND DISCUSSION

Geometry optimization

Taking the standard geometric parameters (Medjani *et al*., 2015), initial geometry was minimized without any constraints to the potential energy surface. These optimized parameters were used for vibrational frequency calculation to characterize all stationary points as minima. The ground state optimized structure of the molecule is as shown in the figure 1 (b). The optimized structure reproduced is remarkably similar to the experimental one. The calculated parameters (bond length, bond angle and the dihedral angles) are similar to the experimental values. Both the optimized and experimental molecular conformations were compared by superimposing them using a least-square algorithm that minimizes the distance between the corresponding non-hydrogen atoms, as shown in figure 1 (c). For clarity, all the hydrogen atoms were removed. The agreement between the optimized and the experimentally observed structure was excellent showing that optimized structure reproduces the experimentally observed conformation.

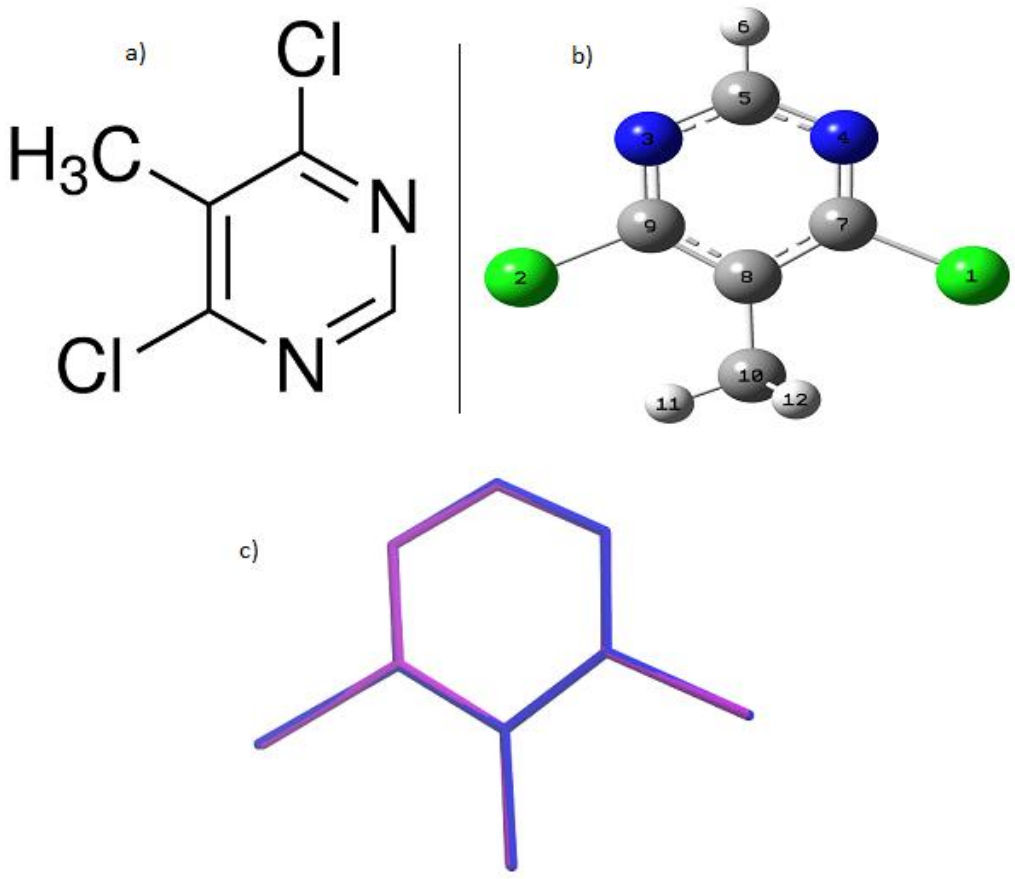

Fig. 1. (a) Crystal structure of DMP, (b) Optimized structure of DMP, and (c) Overlapping between the experimental (purple) and optimized (blue) structures.

The relative minimum energies of the molecule calculated by employing *ab initio* HF functions and B3LYP functional are -1219.64827061 and -1222.97130444 Hartree, respectively. The enthalpy difference between these two theories is 4.07194kcal/mol. Also, a comparison between experimental and optimized hydrogen bond parameters is as shown in the Table 1. The optimized structure of dimer and unit cell are as shown in the figure 2 (a & b).

Table 1. Comparison between the experimental and optimized H-bond parameters.

	D—H----A	D—A (Å)	H....A (Å)	D...A (Å)	D—H...A (^{o})
Expt.	C2—H2..N3^i	0.93	2.66	3.468 (6)	146
Cal.	,,	1.0845	2.6097	3.38428	137

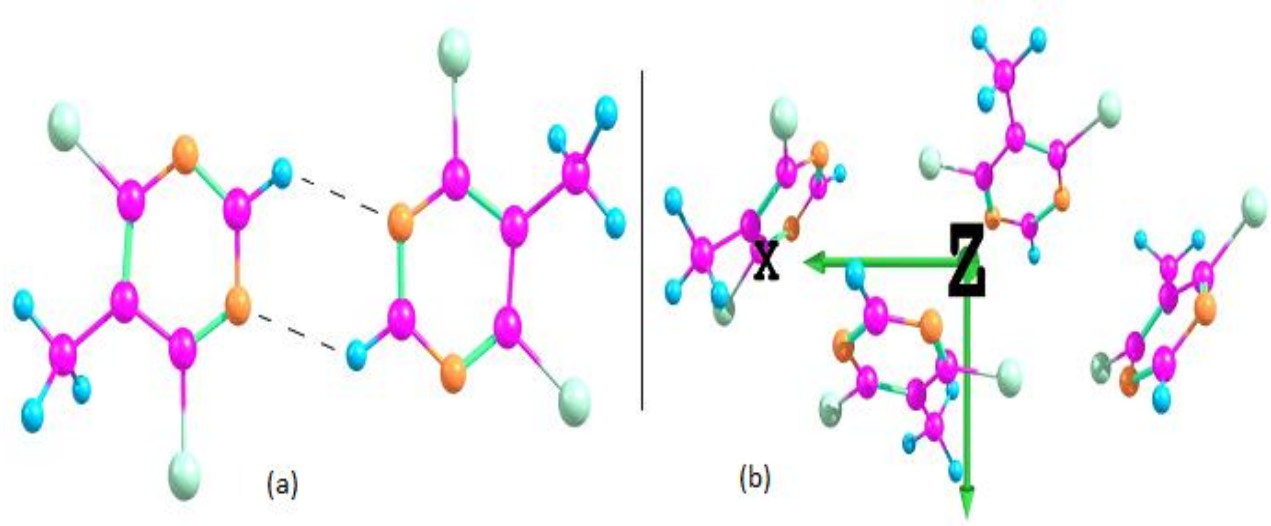

Fig. 2. Optimize structures; (a) dimer and (b) unit cell of DMP molecule.

Molecular electrostatic potential (MEP)

The molecular electrostatic potential (MEP) in a molecule at a point r (x,y,z) is the force on unitary positive test charge at that point due to its whole electrical charge and is given by:

$$V(r) = \sum_A \frac{Z_A}{|\vec{R}_A - \vec{r}|} - \int \frac{\rho(\vec{r'})dr}{|\vec{r'} - \vec{r}|}$$

where Z_A is the charge on nucleus A located at R_A and $\rho(r')$ is the electron density. The first term is due to the nucleus and the second due to electron cloud.

The MEP provides a visual method to understand the relative polarization of molecule (Srivastava *et al*., 2013). Such surfaces depict the size, shape, charge density and site of chemical reactivity of the molecules. In the surface generated, negative electrostatic potential (shades of red color) corresponds to an attraction of the proton by the concentrated electron density in the molecules (from lone pairs, pi-bonds, etc.) and positive electrostatic potential (shades of blue color) corresponds to repulsion of the proton by the atomic nuclei in the regions where low electron density exists and the nuclear charge is incompletely shielded. The largely white or lighter color shades on the surface indicate that the molecule is mostly non-polar. The potential increases in the order red < orange < yellow < green < blue.

Molecular electrostatic potential surface (MEP) of DMP molecule mapped with the output obtained by B3LYP/6-311++G (d, p) is as shown in figure 3. From the figure it is clear that the most negative regions (red regions) are localized over the nitrogen atoms as the sites for nucleophilic reactivity. Similarly, the most positive region (blue region) is localized over the hydrogen atoms of methyl group which is expected to be electrophilic regions.

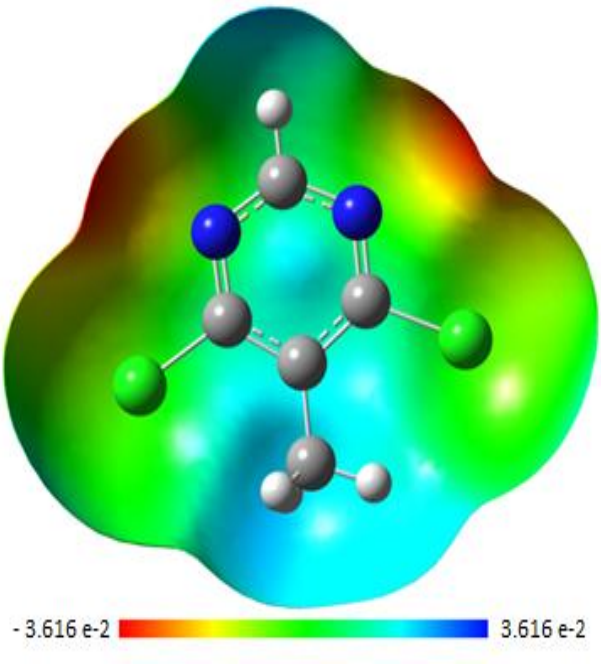

Fig. 3. Molecular electrostatic potential mapped.

Electronic absorbance and HOMO-LUMO band gap

The frontier molecular orbitals characterized by HOMO (highest occupied molecular orbital) and LUMO (lowest unoccupied molecular orbital) are the most significant orbitals in a molecule. These orbitals play vital role in predicting electric and optical properties. The energy of the HOMO is directly related to the ionization potential and the energy of the LUMO is directly related to the electron affinity. Higher gap energy (ΔE) indicates more stability of molecule and vice versa. Usually, a molecule with small frontier gap is more optically polarizable, kinetically less stable, has high conductivity and high reactivity in chemical reactions (Lewis *et al*., 1994). The calculated electronic absorption spectra in both the gas and solvent phase (DMSO; Dimethyl sulphoxide) using time dependent density functional theory (TD-DFT) employing 6-31G (d, p) basis set is shown below in the figure 4.

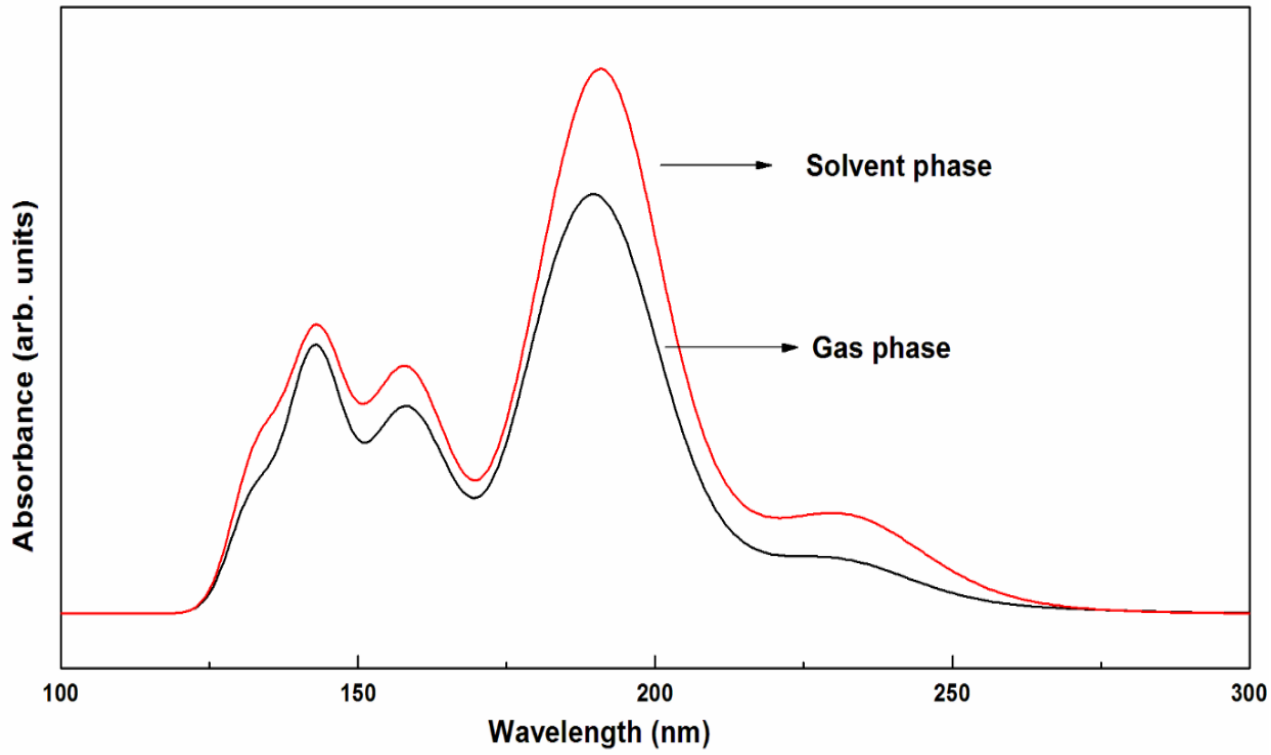

Fig. 4. UV-Vis absorption spectrum of the title molecule.

The calculated frontier orbital energies, absorption wavelengths (λ_{max}), oscillator strengths (f), excitation energies (E), and dipole moments (μ) for gas as well as the solvent phase are illustrated in table 2. The electronic absorption corresponds to the transition of an electron from the HOMO (referred as ground state) to the LUMO (as first excited state).

Table 2. Electronic transitions, absorption wavelength λ_{max} (nm), excitation energy (eV), oscillator strengths (f), frontier orbital energies (eV) and dipole moment (Debye).

Excited State	Gas phase				Solvent (DMSO) phase			
	λ_{max} (nm)	Transitions	E(ev)	Oscillator strength (f)	λ_{max}(nm)	Transitions	E(ev)	Oscillator strength (f)
1	263.49	H→L	4.7055	0.0044	258.15	H-1→L	4.8028	0.0050
2	231.08	H-1→L	5.3654	0.0559	232.63	H→L	5.3297	0.1018
3	209.04	H-1→L+1	5.9311	0.0380	209.86	H→L+1	5.9079	0.0636
4	199.72	H-3→L	6.2080	0.0049	196.48	H-4→L+1	6.3103	0.0049
5	193.87	H-2→L	6.3951	0.1464	193.89	H-2→L	6.3946	0.2070
6	192.78	H-2→L+1	6.4315	0.1945	191.98	H-2→L+1	6.4583	0.2981
7	182.11	H→L+2	6.8082	0.2394	181.19	H-1→L+2	6.8428	0.2251
8	158.09	H-3→L+2	7.8424	0.0450	157.27	H-3→L+2	7.8837	0.0520
9	156.35	H→L+3	7.9299	0.1205	155.97	H-1→L+3	7.9494	0.1373
10	143.38	H-7→L+1	8.6470	0.1184	143.70	H-7→L	8.6282	0.1944
11	142.67	H-7→L	8.6903	0.1654	142.79	H-7→L+1	8.6832	0.0911

	E_{HOMO} (eV)	E_{LUMO} (eV)	ΔE (eV)	μ(D)
Gas	-6.687113	-1.607280	5.079833	1.4808
Solvent	-7.655984	-1.580368	5.979472	1.9121

HOMO=41, LUMO=42

The first allowed transition (H→L) in gas phase was calculated at 263.49 nm with oscillator strength 0.0044 and in solvent phase it was at 258.15 nm (H-1→L) with oscillator strength 0.050. The other main transitions in the gas phase were calculated at 231.08 nm (H-1→L), 192.78 nm (H-2→L+1), 182.11 (H→L+2), 156.35 (H→L+3) and 142.67 nm (H-7→L) with oscillator strengths 0.0559, 0.1945, 2394, 0.1205 and 0.1654, respectively. Similarly, in the solvent phase the main transitions were at 232.63 (H→L), 191.98 (H-2→L+1), 181.19 (H-1→L+2), 155.97 (H-1→L+3) and 143.70 nm (H-7→L) with the oscillator strengths 0.1018, 0.2981, 0.2251, 0.1373 and 0.1944, respectively. DMSO being a polar aprotic solvent, increases the polarity of the molecule as such the calculated dipole moment in the solvent phase (1.9121) is higher than in the gas phase (1.4808). Similarly, the energy difference ($\Delta E = E_{LUMO} - E_{HOMO}$) between the two molecular orbitals was 5.079833 and 5.979472 eV, respectively in the solvent and gas phases.

Figure 5 shows HOMO-LUMO plot for the different molecular orbitals taking part in the charge accumulation process in the gaseous phase. The red regions indicate to the positive charge and blue regions to the negative charge accumulating parts of the molecule. In HOMO, charge is accumulated from nitrogen and chlorine molecules together with the charge from ring, while in LUMO the charge accumulation occurred at the ring elements (nitrogen and carbon). In HOMO-1 and HOMO-2 the charge is mainly accumulated from the ring and chlorine atom while in case of LUMO+1 almost the charge is accumulated at the ring elements. In HOMO-7 the charge accumulation is dominated by the lone-pair elements. In this molecule main transition types are $\pi \rightarrow \pi^*$ in the ring and and $n \rightarrow \pi^*$ (in the lone-pair elements).

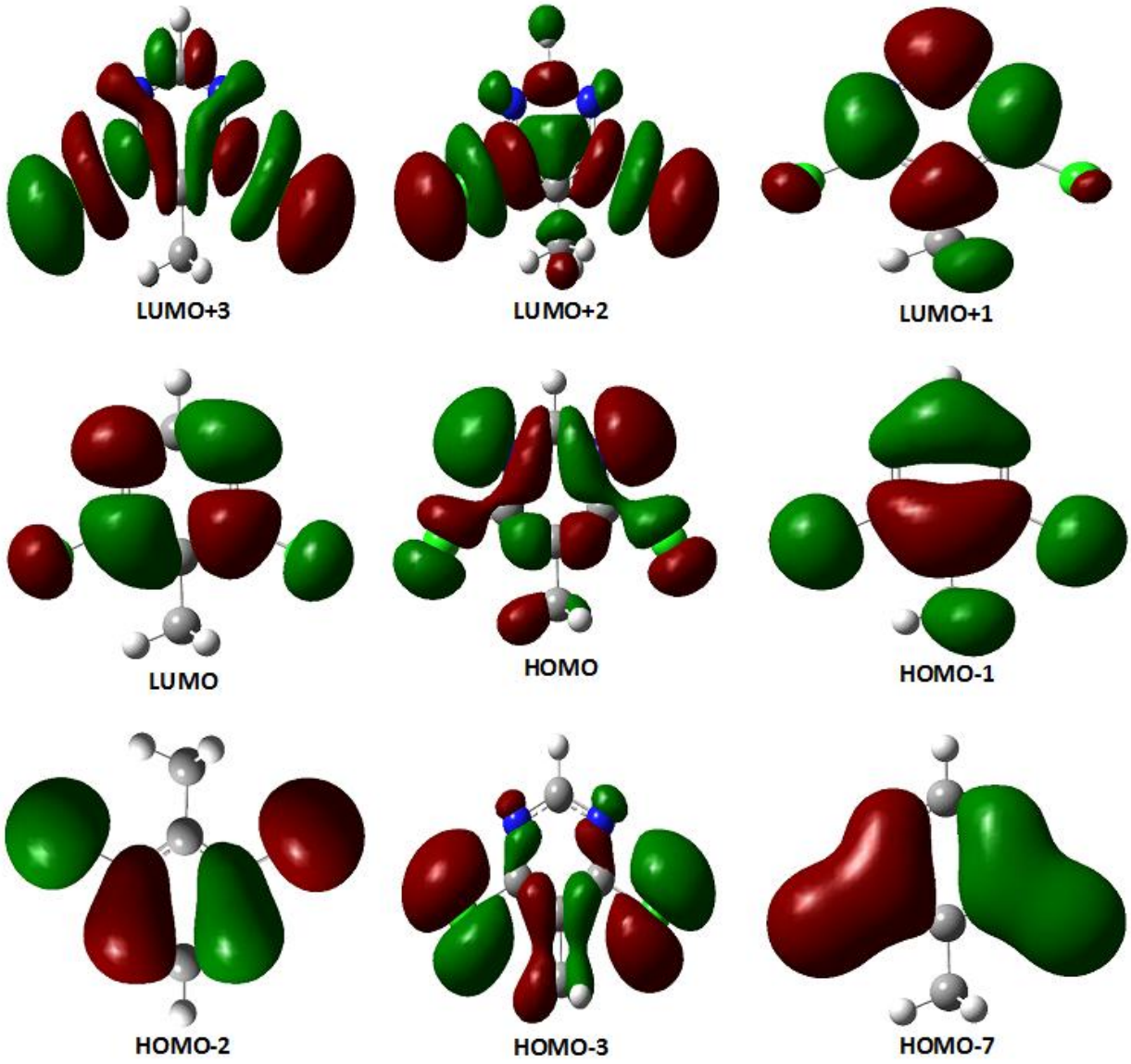

Fig. 5. Plots of HOMOs and LUMOs of DPN molecule showing the charge accumulation.

Vibrational frequencies

DMP molecule has 13 atoms, hence it gives 33 (3N-6; N is the number atoms) modes of vibrations. All the frequencies / wavenumbers are both Raman and IR active. The calculated frequencies (for monomer, dimer and unit cell) have been scaled by the wavenumber linear scaling (WLS) of Yoshida *et al*. 2002 using the expression: υ_{obs} = (1.0087-0.0000163 υ_{cal}) υ_{cal}. The calculated frequencies of DMP molecule for its monomer, dimer and unit cell level are listed in the Table 3. The Raman and IR spectra are shown in the figure 6 and 7, respectively. Further, a brief assignment of these frequencies according as the numbering system as shown in figure 6 is given below:

Methyl vibration

CH_3 group has several modes associated with it, such as symmetric and asymmetric stretches, bends, rocks, and torsional modes. In this study, the asymmetric stretching was calculated at 3020 and 2962 cm^{-1} in the monomer. This vibration has same values in the dimer while there was small difference in unit cell. Symmetric vibration related to this group was at 2919 cm^{-1}, which was strong in the Raman and weak in the IR band. The deformation vibrations of CH_3 were calculated at 1465 and 1462 cm^{-1}.

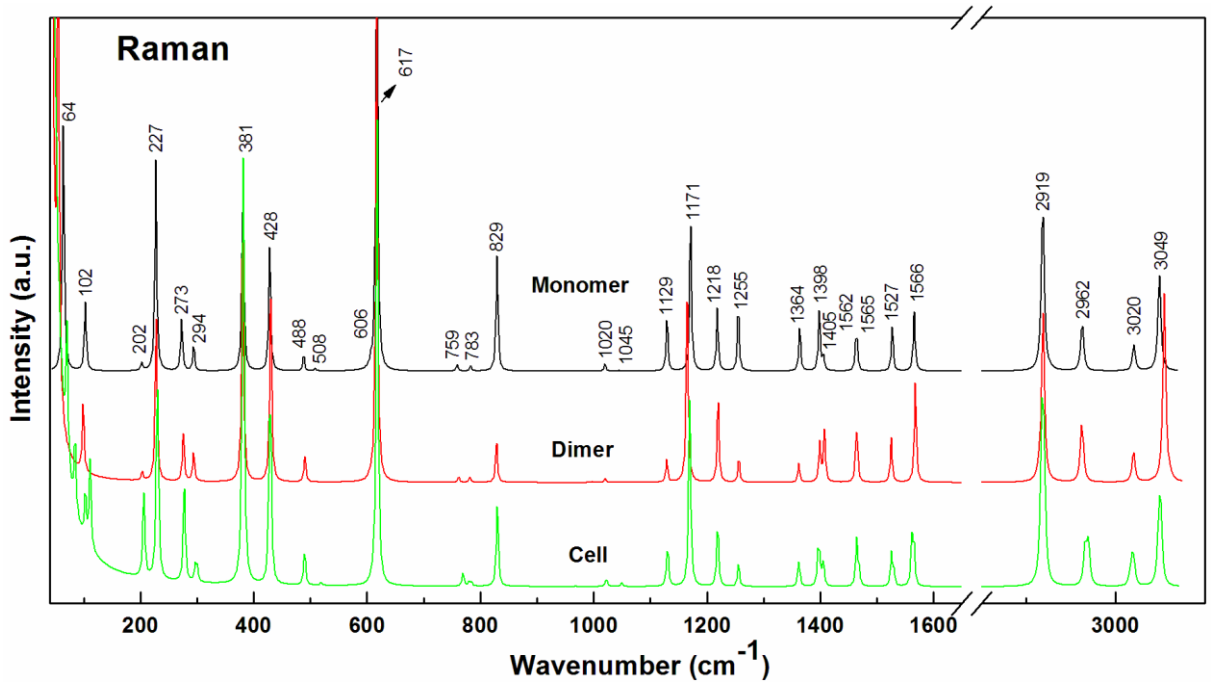

Fig. 6. Calculated Raman spectra.

Pyrimidine ring vibration

There are two chlorides, one methine and a methyl group as functional groups attached to the pyrimidine ring. C-H stretching vibration was calculated at 3049 / 3211 cm^{-1} in the scaled DFT/HF, respectively. The in-plane deformation vibration for monomer was at 1405 cm^{-1} in DFT and at 1529 cm^{-1} in the HF method. The two values of this mode in the dimer are 1409 and 1407 cm^{-1}. Similarly, the four values of the in-plane deformation in the cell are 1407, 1406, 1405 and 1405 cm^{-1}, respectively. C-H out-of-plane vibration for monomer was at 927 cm-1 in DFT.

This mode was calculated respectively at 997/ 994 cm^{-1} in the dimer and at 969,969,968 and 968 cm^{-1} in the cell.

C-Cl stretching vibration was calculated at 428 / 381 cm^{-1} in DFT and 471 / 416 cm^{-1} in the HF. This vibration has been obtained in the range 430-380 cm^{-1} in case of both the dimer and unit cell. The in-plane vibration of C-Cl mode was at 227 cm^{-1} in DFT method.

Table 3. Calculated wave numbers (in cm^{-1}) of DMP for its monomer, dimer and unit cell.

Unscaled	Scaled wave numbers				PED[a] distribution (%)
	Monomer		Dimer	Cell	
DFT	HF	DFT	DFT		
3187	3211	3049	3055, 3053	3051,3051,3049,3049	υ(CH)(99)
3155	3161	3020	3020, 3020	3020,3020,3018,3018	$\upsilon_a(CH_3)$(99)
3091	3101	2962	2962, 2962	2969,2969,2966,2966	$\upsilon_a(CH_3)$(100)
3043	3053	2919	2918, 2918	2920,2920,2918,2918	$\upsilon_s(CH_3)$(100)
1593	1730	1566	1568,1564	1565,1565,1563,1531	υ(C=N)(46)+υ(CC)(24)+R[$\delta_{a'}$](8)+υ(CN)(8)+ υ(C8C10)(5)
1553	1707	1527	1528,1525	1530,1530,1527,1525	υ(CN)(38)+δ_{in}(CH)(16)+υ(CC)(26)+R[δ_a](6)
1488	1585	1465	1465, 1465	1469,1469,1465,1465	[δ_a(81)+ρ'(8)](CH3)

1485	1583	1462	1464, 1463	1464,1464,1463,1463	$[\delta_{a'}(69)+\rho(8)](CH_3)+\delta_{in}(CH)(10)$
1426	1529	1405	1409,1407	1407,1406,1405,1405	$\delta_{in}(CH)(34)+\delta_s(CH_3)(31)+\upsilon(CC)(11)+\upsilon(C=N)(9)$
1419	1523	1398	1400,1400	1399,1399,1396,1396	$\delta_s(CH_3)(67)+\delta_{in}(CH)(13)+\upsilon(C8C10)(5)$
1383	1481	1364	1362,1361	1364,1364,1363,1361	$\upsilon(C8C10)(21)+\upsilon(CC)(30)+\upsilon(CN)(29)+\upsilon(C=N)(9)$
1270	1364	1255	1256,1248	1257,1256,1255,1254	$\upsilon(CN)(42)+\upsilon(CC)(20)+\delta_{in}(C8C10)(11)+\delta_{in}(CH)(8)+\rho(CH_3)(7)$
1232	1273	1218	1233,1230	1220,1219,1218,1217	$\upsilon(C=N)(56)+\upsilon(CC)(17)+\upsilon(CN)(16)+\delta_{in}(CH)(6)$
1183	1231	1171	1169,1165	1171,1170,1170,1169	$\upsilon(CN)(45)+\upsilon(C=N)(20)+R[\delta_{trig}](12)+\upsilon(C8C10)(10)+\upsilon(C=N)(6)$
1140	1169	1129	1129,1128	1132,1131,1129,1129	$R[\delta_{trig}](52)+\upsilon(C8C10)(16)+\upsilon(CN)(18)$
1054	1145	1045	1046, 1046	1049,1049,1047,1047	$[\rho'(78)+\delta_a(6)](CH_3)+\delta_{out}(C8C10)(7)$
1028	1099	1020	1020, 1020	1024,1023,1022,1021	$\rho(CH_3)(63)+\upsilon(CC)((13)+\upsilon(CN)(9)$
979	1085	972	997, 994,	969,969,968,968	$\delta_{out}(CH)(91)+R[puck](5)$
833	903	829	828, 828	831,831, 830,830	$R[\delta_{a'}(34)+\delta_{trig}(19)]+\upsilon(C8C10)(17)+\upsilon(CCl)(13)+\upsilon(CC)(9)$
786	853	783	783, 781	785,785, 781,780	$R[\delta_a](41)+\upsilon(CCl)(40)+\upsilon(CC)(10)$
762	844	759	762, 762	770,770, 769,768	$R[puck](62)+\delta_{out}(CCl)(27)+\delta_{out}(C8C10)(8)$
618	677	617	617,617	618,618, 618,618	$R[\delta_{a'}](34)+\upsilon(C8C10)(25)+\upsilon(CCl)(19)+\upsilon(CC)(9)+\upsilon(CN)(7)$
607	660	606	605,604	611,610, 609,609	$R[\tau_a](75)+\delta_{out}(CCl)(35)$
508	559	508	516, 509	519,519, 518,518	$R[\tau_{a'}](44)+\delta_{in}(C8C10)(32)+\delta_{out}(CCl)(19)$
488	530	488	490, 490	491,490, 489,489	$\delta_{in}(C8C10)(35)+\delta_{in}(CCl)(32)+R[\delta_a](15)+\upsilon(CN)(7)+\rho(CH_3)(5)$
427	471	428	430, 427	430,430, 428,428	$\upsilon(CCl)(40)+\upsilon(CN)(30)+R[\delta_a](20)+\delta_{in}(C8C10)(6)$
380	416	381	380, 380	382,382, 380,380	$\upsilon(CCl)(31)+\upsilon(CN)\ (29)+R[\delta_{a'}(21)+\delta_{trig}(8)]$
293	317	294	294, 294	300,300, 297,297	$\delta_{in}(C8C10)(47)+\delta_{in}(CCl)(42)+R[\delta_a](6)$
271	299	273	375,374	278,277, 277,277	$\delta_{out}(C8C10)(55)+\delta_{out}(CCl)(38)$
226	245	227	228,227	231,231, 228,228	$\delta_{in}(CCl)(86)+\upsilon(CC)(6)$
201	230	202	203,203	207,207, 206,205	$R[\tau_a](90)+\delta_{out}(CCl)(11)$
102	120	102	99,99, 55,45	111,111, 104,103, 85,84,70,69	$\tau(C8C10)(55)+R[\tau_{a'}](26)$
63	75	64	31, 31, 17,13,7	41,39,31,29,29,28,28, 27,22,21, 20,19,17, 16,14,9,9,5	$\tau(C8C10)(46)+R[\tau_{a'}(32)+puck(9)]$

(Proposed assignments and potential energy distribution (PED) for vibrational normal modes. Types of vibration: ν, stretching; δ, deformation (bending), scissoring; oop, out-of-plane bending; ω, wagging; γ, twisting; ρ, rocking; τ, torsion; [a]Potential energy distribution (contribution ≥ 5)).

C8-C10 stretching vibration was calculated at 1364 cm^{-1} in the scaled DFT and at 1481 cm^{-1} in HF method. The in-plane and out-of-plane vibrations of C8-C10 were at 294 and 273 cm^{-1}, respectively.

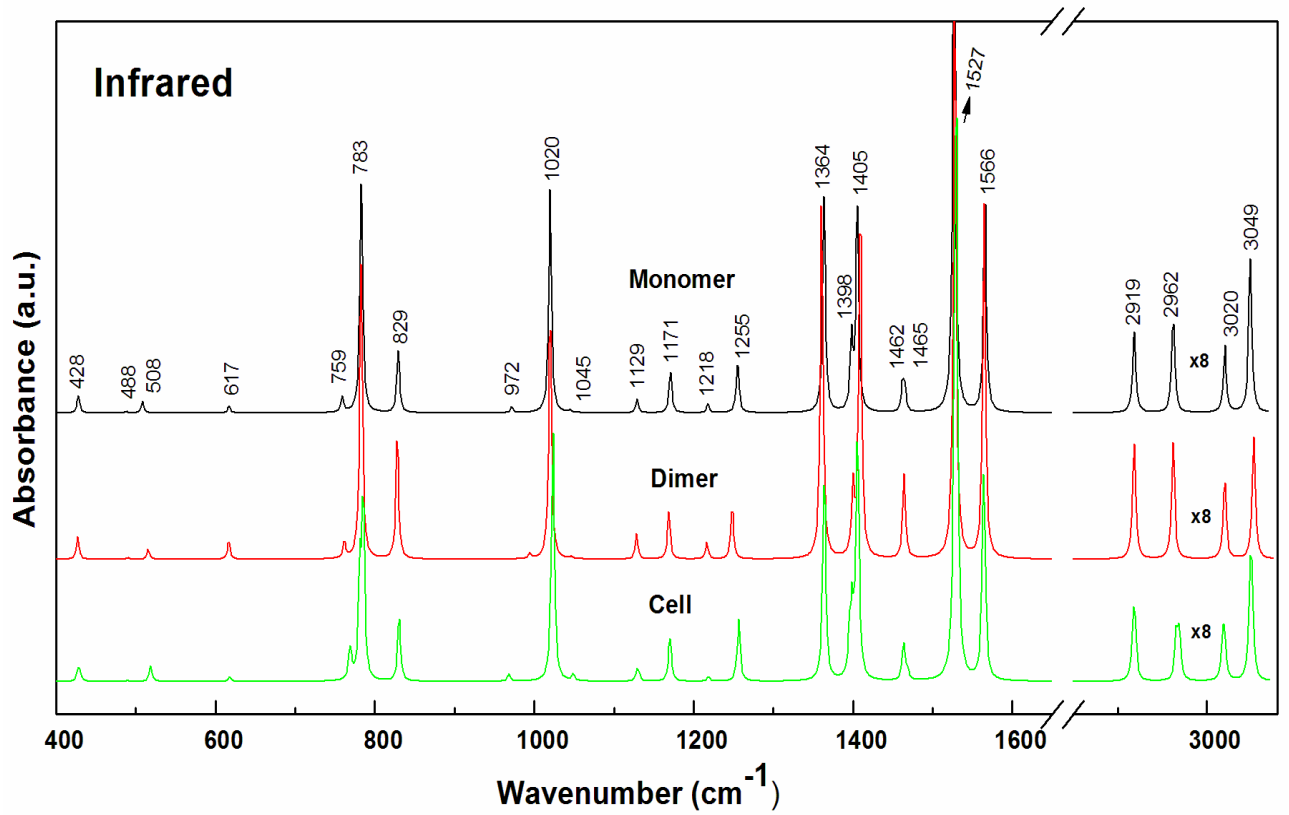

Fig. 7. Calculated infrared spectra.

CONCLUSION

The equilibrium geometries and harmonic vibrational wave numbers of all the 33 normal modes, the monomer, 72 normal modes of dimer and 150 normal modes of unit cell of DPN molecule were determined and analyzed both at DFT (B3LYP) theory employing the 6-311++G (d, p) basis set. These spectra are in good agreement. These vibrational assignments along with the electronic transitions are important to understand the molecular structure of the title molecule. The H-bond length of 2.6093 Å between the two molecules of dimer indicates that the molecular system is governed by strong H-bonding in its packing. The MEP plot shows that the regions near the nitrogen and chlorine atoms are most electronegative while the regions near the hydrogen atoms are most electro positive. The frontier energy gap is higher in the solvent phase than in the gas phase. The HOMO-LUMO plot notices that the charge transfer takes place within the molecule.

ACKNOWLEDEGEMENTS

The Brazilian National Council for Scientific and Technological Development (CNPq) and TWAS, the academy of sciences for the developing world (CNPq-TWAS/Post-Doc fellowship (2014) are highly acknowledged.

REFERENCES

Alam, O.; Khan, S. A.; Siddiqui, N. and Ahsan, W. (2010). *Medicinal Chemistry Research,* **19** (9): 1245–1258.

Becke, A. D. (1993). Density-functional thermo chemistry. III. The role of exact exchange. *Journal of Chemical Physics*, **98**: 5648-5652.

Casida, M. E. and Chong, D. P. (eds.) (1995). *Recent Developments in Density Functional Theory*. World Scientific, Singapore, **1**: 155.

Casida, M. E.; Casida, K. C. and Salahub, D. R. (1998). Excited-state potential energy curves from time-dependent density-functional theory: A cross section of formaldehyde's 1A1 manifold, *International Journal of Quantum Chemistry*, **70** (4-5): 933-941.

Condon, M. E.; Brady, T. E.; Feist, D.; Malefyt, T.; Marc, P.; Quakenbush, L. S. *et al*., (1993). *Brighton Crop Prot. Conf. Weeds*, BCPC Publications, Alton, Hampshire, England, pp. 41–46.

Frisch, A.; Nielson, A. B. and Holder, A. J. (2000). Gauss View User Manual, Gaussian Inc, Pittsburgh, P.A.

Frisch, M. J.; Trucks, G. W.; Schlegel, H. B.; Scuseria, G. E.; Cheeseman, J. R.; Robb, M. A. et al. (2009). *GAUSSIAN 09, Revision, Gaussian Inc*. Wallingford, CT.

Hohenberg, P. and Kohn, W. (1964). "Inhomogeneous Electron Gas", *Physical Review B*, **136**: 864-871.

Khidre, R. E. and Abdel-Wahab, B. F. (2013). Application of Benzoylaceteonitrile in the Synthesis of Pyridines Derivatives, *Current Organic Chemistry*, **17** (2): 1-16.

Lee, C. T.; Yang, W. and Parr, R. G. (1988). "Development of the Colle-Salvetti correlation-energy formula into a functional of the electron density". *Physical Review B*, **37** (2): 785-789.

Lewis, D. F. V.; Ioannides, C. and Parke, D. V. (1994). Interaction of a series of nitriles with the alcohol-inducible isoform of P450: Computer analysis of structure—activity relationships, *Xenobiotica*, **24** (5): 401-408.

Maeno, S.; Miura, I.; Masuda, K. and Nagata, T. (1990). *Brighton Crop Protection Conference on Pests and Diseases*, BCPC Publications, Alton, Hampshire, England, pp. 415-422.

Martin, J. M. L. and Aslenoy, C. V. (1995). Gar2ped. University of Antwerp. Belgium.

Medjani, M.; Hamdouni, N.; Brihi, O.; Boudjadaa, A. and Meinnel, J. (2015). Crystal structure of 4, 6-dichloro-5-Methylpyrimidine, *ActaCryst E (crystallographic communication),* **71**: 01073–01074.

Mishra, R.; Joshi, B. D.; Srivastava, A.; Tandon, P. and Jain, S. (2014). Quantum chemical and experimental studies on the structure and vibrational spectra of an alkaloid–Corlumine, *Spectrochimica Acta A*, **118**: 470-480.

Parr, R. G. and Yang, W. (1989). *Density Functional Theory of Atoms and Molecules.* Oxford University Press, New York. Oxford, pp 333.

Selby, T. P.; Drumm, J. E.; Coats, R. A.; Coppo, F. T.; Gee, S. K.; Hay, J. V.; *et al.* (2002). *Synthesis and Chemistry of Agrochemicals, ACS Symposium Series, American Chemical Society*, Washington DC, **800**: 74-84.

Srivastava, A.; Mishra, R.; Tandon, P. and Bansal, A. K. (2013). FT-Raman, FT-IR, UV spectroscopic, NBO and DFT quantum chemical study on the molecular structure, vibrational and electronic transitions of clopidogrel hydrogen sulfate form 1: A comparison to form 2, *Spectrochimica Acta A*, **104**: 409-418.

Yoshida, H.; Takeda, K.; Okamura, J.; Ehara, A. and Matsurra, H. (2002). A New Approach to Vibrational Analysis of Large Molecules by Density Functional Theory: Wave number-Linear Scaling Method, *Journal 0f Physical Chemistry A*, **106**: 3580-3586.